Temporal characterization of attosecond wave forms in the sub-optical-cycle regime

Isabell Thomann,[1,][*] Emily Gregonis,[1] Xuan Liu,[2] Rick Trebino,[2] Arvinder S. Sandhu,[1]
Margaret M. Murnane,[1] and Henry C. Kapteyn[1]

[1]*JILA, University of Colorado and NIST, Boulder, Colorado 80309, USA*
[2]*School of Physics, Georgia Institute of Technology, Atlanta, Georgia 30332, USA*
(Received 3 May 2007; revised manuscript received 28 May 2008; published 24 July 2008)

We present a temporal characterization of sub-optical-cycle extreme ultraviolet radiation generated in a hollow-core waveguide. This generation scheme permits the use of relatively long 13-fs driving laser pulses to generate sub-optical-cycle bursts of high-order harmonic light. Using two-color cross-correlation and phase retrieval techniques, we extract the extreme ultraviolet wave form and show that it consists of chirped 470-as bursts, spaced by $\sim$1.3 fs, within a 1.4-fs intensity envelope. The radiation is spectrally narrow and energy tunable, making it a useful tool to investigate state-selective molecular and materials dynamics.

High-order harmonic up-conversion of intense femtosecond laser light results in a tabletop-scale source of coherent light in the extreme ultraviolet (EUV) region of the spectrum. This light source has produced the shortest light pulses measured to date, making it ideal for observing dynamics in atoms, molecules, and materials on femtosecond (fs $=10^{-15}$ s) or attosecond (as$=10^{-18}$ s) time scales. In general, high-order harmonic generation (HHG) produces a train of attosecond bursts, with an interpulse spacing corresponding to half of the fundamental driving laser period. Under specific conditions, either trains of attosecond pulses or isolated attosecond bursts can be produced [1–5]. To date, considerable effort has been devoted to generating isolated attosecond EUV pulses using very short, 5-fs, carrier-envelope-phase stabilized driving laser pulses [5]. Such ultrashort laser pulses need meticulous dispersion control over a large frequency bandwidth and are challenging to propagate through even 1 m of air (which will broaden a 5-fs pulse to 12 fs). Moreover, the EUV spectrum that supports an isolated attosecond pulse consists of a broad continuum. However, many experiments in ultrafast molecular and materials spectroscopy require EUV pulses slightly longer in duration, in the range of $\sim$1 fs. This is because such pulses can have a sufficiently narrow spectral bandwidth to either initiate or probe the femtosecond dynamics of specific electronic excited states with reasonable spectroscopic resolution ($\sim$1 eV). Good spectroscopic resolution is required for obtaining initial-state-specific photoelectron spectra in the typically congested EUV spectra of molecules, molecular clusters, or solids [6–12]. Therefore, the generation and characterization of sub-optical-cycle EUV pulses with narrow spectral bandwidth is a topic of great interest that is unexplored to date.

Generating and characterizing sub-optical-cycle EUV wave forms is challenging. Nearly all current EUV pulse characterization techniques rely on two-color photoionization, in which an atom is simultaneously irradiated with EUV and near-infrared (NIR) laser fields and the energy of the resultant electrons is monitored as a function of the time delay between the laser and EUV fields. In the case of rela-

tively long EUV pulses ($>$10 fs), the EUV pulse duration can be deconvolved from the cross correlation measurement provided that the laser pulse duration is accurately characterized. However, in order to extract the pulse duration of a sub-optical-cycle EUV field from a cross correlation measurement, both the laser pulse and the cross correlation between the EUV and laser fields would need to be measured to an accuracy better than $\sim$0.05 fs (which is not feasible). The reconstruction of attosecond beating by interference of two-photon transitions (RABBIT) technique [13] can be used to determine the temporal structure of the individual attosecond bursts—but not the overall envelope. Alternatively, the frequency-resolved optical gating for complete reconstruction of attosecond bursts (FROGCRAB) technique [14] has recently been introduced, which in theory allows for reliable deconvolution of an EUV wave form of any duration. However, this measurement technique has to date been applied only to the case of a single isolated EUV burst of 130-as duration [5], where the isolated nature of the EUV burst considerably simplifies the pulse shape extraction.

In this work, we present a temporal characterization of sub-optical-cycle EUV pulses generated in a hollow waveguide [15]. This new generation scheme allows us to use significantly longer driving laser pulses, of 13 fs in duration, than have been used for sub-optical-cycle EUV generation to date. Such 13-fs driving pulses can be generated by standard ultrafast laser pulse compression techniques. We use two independent techniques to extract the complex EUV field: an iterative step-by-step reconstruction, based on a constrained number of physical parameters and error minimization between the experimental FROGCRAB trace and a simulation based on the expression given in [14], and an unrestricted FROGCRAB pulse retrieval algorithm. Both methods independently show that the generated EUV pulse consists of a very short train of moderately chirped 470-as pulses, with bursts spaced by $\sim$1.3 fs with the total energy contained within a 1.4-fs full-width at half-maximum (FWHM) pulse envelope. Moreover, we show that the EUV field is near the Fourier-transform limit, with a narrow spectral bandwidth where $\sim$64% of the energy is contained within a single harmonic peak of 1.1 eV FWHM. Finally, the EUV pulse can be tuned over an energy range between 38 eV and 48 eV by adjusting the driving laser intensity and the gas pressure in the waveguide. Because of the sub-optical-cycle pulse dura-
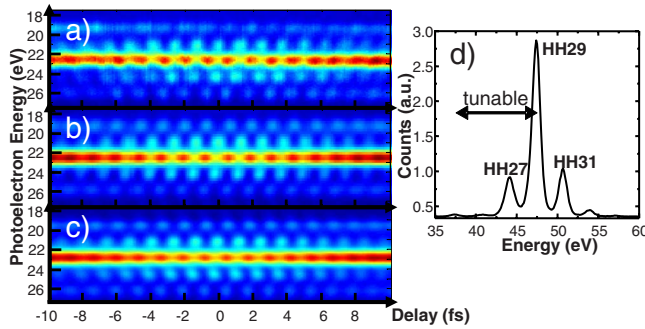
---

*Isabell.Thomann@Colorado.edu

FIG. 1. (Color online) (a) Experimental photoelectron spectrum as a function of time delay between the EUV and IR pulses, when these pulses are focused simultaneously into He gas. (b) FROGCRAB simulation of the data in (a) based on theory presented in [14]. (c) FROGCRAB trace obtained from a generalized projections (GP) algorithm. (d) EUV spectrum of the pulse that generated the photoelectron spectrum shown in (a). The energy tuning range is indicated.

tion, narrow bandwidth, ease of tunability, and greatly simplified generation scheme, this source will have many applications in probing electron dynamics with state selectivity in molecular systems and materials.

Our experiment starts with 30-fs laser pulses from a cryogenically cooled 2-kHz Ti:sapphire laser amplifier, similar to the ultrafast laser amplifier systems present in hundreds of laboratories worldwide. We use a 1-m-long, 400-μm-diameter hollow-core waveguide filled with argon gas to broaden the laser spectrum and temporally compress the pulses using commercially available negative chirped mirrors. We then focus the 13-fs, 2×10^{14}-W cm^{-2} pulses into a 2.5-cm-long, 150-μm-diameter hollow-core waveguide [16] filled with argon gas, in which the high-order harmonic radiation is generated. To temporally characterize the EUV pulse, we employ an interferometric EUV-NIR cross correlation geometry [17]. The EUV and fundamental driving pulse are focused into a helium gas jet, and a cross-correlation signal is obtained from the generated photoelectron spectra as the relative delay between the two pulses is varied. The delay line makes use of the different divergences of the fundamental and the EUV beam. The low-divergence, central EUV beam passes through a small circular Al filter suspended in a nitrocellulose filter. The annular fundamental beam, which passes around the Al filter, is reflected by an annular mirror, while the central EUV beam is reflected by a Mo/Si mirror that is mounted on a piezoelectric transducer to introduce a variable delay between the fundamental beam and the EUV beam. The Mo/Si mirror reflectivity is centered at ~47 eV with a FWHM ~13 eV, so that all harmonics generated in the waveguide are reflected. The photoelectrons ejected from helium by the EUV beam are then detected using a magnetic bottle time-of-flight spectrometer and a multichannel plate (MCP) detector. This spectrometer has a 2π detection solid angle; i.e., photoelectrons parallel and perpendicular to the laser polarization (which points towards the MCP) are detected.

Figure 1(a) shows the experimental cross-correlation data. At large time delays between the EUV and NIR pulses, the

photoelectron spectra are generated by the EUV light alone. The photoelectron peak generated by the dominant harmonic is clearly visible, as well as two adjacent smaller photoelectron peaks generated by the two adjacent weaker harmonics. When both EUV and fundamental beams are present, sidebands occur due to the absorption of an EUV photon simultaneous with absorption or emission of a fundamental photon. The sidebands are modulated at a period corresponding to half the fundamental laser cycle. In the following, we use the FROGCRAB technique for a careful analysis of our data. The FROGCRAB technique is based on the well-established FROG technique for measuring ultrashort laser pulses in the NIR-visible region, where a temporal gate is used to measure the spectrum of each temporal slice [18]. The temporal gate for FROG is usually an amplitude gate. Instead of an amplitude gate, the FROGCRAB technique uses the fundamental field as a phase gate that modulates the electron wave packet ionized by the EUV beam. It is established that for most conventional FROG techniques [18], spectrograms will have a certain shape depending on the phase of the E field to be measured. One might expect that the phase gate used in the FROGCRAB technique might generate nonintuitive traces [14]. However, as we show below, this is not the case.

First, to gain intuitive insight into the properties of the generated radiation, as well as in the characteristic features of the FROGCRAB trace, we perform an iterative error minimization between the experimental FROGCRAB trace and a simulation. The results of this first analysis will be later fully confirmed by a second, independent analysis using an unrestricted pulse retrieval algorithm. To generate simulated FROGCRAB traces, we employed the strong-field-approximation expression given in [14]. We adapted it to our experimental case where photoelectrons are detected over a 2π solid angle by averaging the photoelectron distribution for different angles including both a geometrical weighting as well as the differential partial cross section for detecting photoelectrons from helium. Our FROGCRAB trace is the addition of two traces for the fundamental light: a cosine and minus cosine wave form. The reason is that we do not need phase-stabilized laser pulses, and the conditions for generating high-order harmonics (phase matching and recollision) are the same for both wave forms. For each delay step, photoelectrons are acquired for multiple laser shots and therefore can contain signal from both wave forms.

Before turning to a detailed analysis of our EUV radiation using the FROGCRAB technique, we first show that, although the FROGCRAB technique uses a seemingly complex phase modulation gate, considerable intuition about pulse characteristics can be obtained from the shape of the sidebands. To demonstrate this, we apply individual dispersion orders to artificially constructed EUV bursts, similar to those generated in our experiment. Sample results of FROGCRAB traces are shown in Fig. 2, plotted over a delay range of two fundamental laser cycles. Figures 2(a)–2(c) show that the shape of the sidebands changes significantly depending on whether second-order phase $D2$ [Fig. 2(a)], third-order phase $D3$ [Fig. 2(b)], or fourth-order phase $D4$ [Fig. 2(c)] is added. FROGCRAB traces can also indicate the sign of the dispersion order, because for opposite signs of dispersion, the sidebands are inverted along the time delay axis.
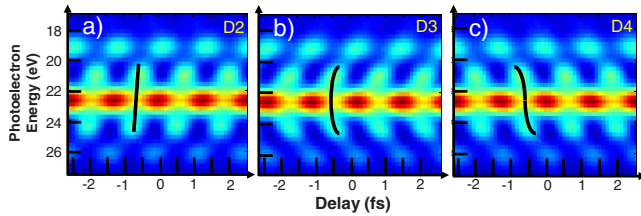
FIG. 2. (Color online) Simulated FROGCRAB data, when higher dispersion orders are artificially introduced into the EUV field: (a) second-order $D2$, (b) third-order $D3$, and (c) fourth-order $D4$ dispersion. Intuitively, the sideband shape shows the group delay of the EUV light, indicated by black lines.

We now turn to a detailed analysis of our experimental FROGCRAB data. To construct the EUV electric field for the simulated FROGCRAB trace, we start with the EUV spectrum shown in Fig. 1(d), recorded using an x-ray spectrometer and charge-coupled-device (CCD) camera. This EUV spectrum is then deconvolved with the Gaussian x-ray spectrometer resolution function of 0.38 eV FWHM, determined by a separate measurement using spectrally narrow harmonics. (Using the measured EUV spectrum without deconvolution would underestimate the pulse duration by ~5%.) The deconvolved EUV spectrum is then multiplied by the transfer functions that relate the measured EUV spectrum to that incident on the detection gas. A spectral phase, described below, is added to the EUV spectrum $E(\omega)$, before transforming into the time domain. The calculated FROGCRAB trace is finally convolved with the measured photoelectron spectrometer resolution function of width ΔE =0.7 eV. This photoelectron spectrometer resolution ΔE imposes an upper limit of approximately $h(0.44/\Delta E)$ (h is Planck's constant) on the envelope duration that can reliably be measured. With the current resolution, we can characterize pulse durations up to 2.5 fs.

As shown above, we can retrieve higher order spectral phases with the FROGCRAB technique. Therefore, in Fig. 3(a), we vary the second-order phase and compare the rms deviation of the experimental and calculated FROGCRAB trace within the central two NIR field cycles. We obtain a second-order phase of $D2=-0.033$ fs^2. Using the same procedure we obtain a minimum rms deviation for third-order dispersion at $D3=-0.007$ fs^3 in Fig. 3(b). The atomic phase of the detection gas, as well as contributions from the EUV mirror and the Al filters, is negligible at the EUV energies considered. Using the best values for the second- and third-order dispersions found in this way, we construct the simulated FROGCRAB trace, shown in Fig. 3(e). This agrees very well and in detail with the experimental trace in Fig. 3(d). The full simulated FROGCRAB trace is shown in Fig. 1(b) and compares excellently with the experimental trace shown in Fig. 1(a).

With the above analysis, we can now plot the correct chirped EUV electric field envelope, shown as the dashed green line in Fig. 4(a). For comparison, the transform-limited electric field envelope is also shown as the dotted red line. Figure 4(b) shows the intensity versus time of the chirped EUV pulse (dashed green line), as well as the envelope corresponding to the transform-limited center harmonic for
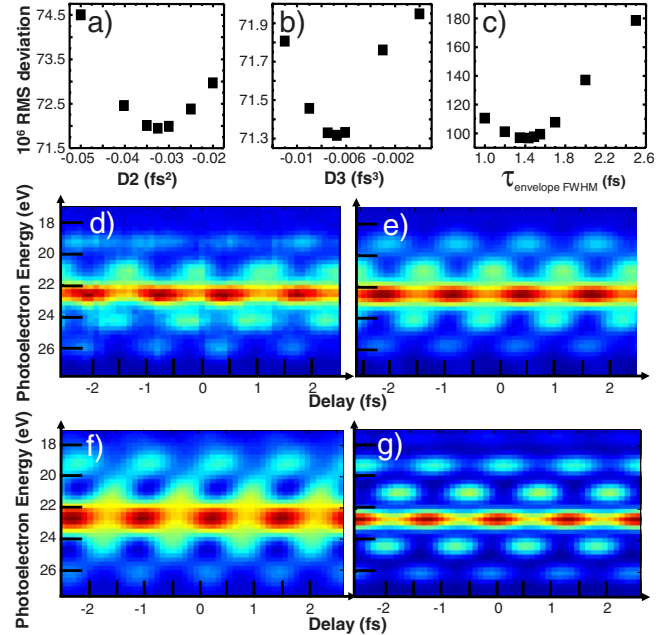

FIG. 3. (Color online) rms deviation between the FROGCRAB simulation and the experimental cross-correlation trace as the parameters of the simulated pulse are varied: (a) Varying the linear chirp $D2$, (b) varying the quadratic chirp $D3$, and (c) varying the EUV pulse envelope. (d) Experimental FROGCRAB data, (e) FROGCRAB data simulated using the optimized values of $D2$, $D3$ and EUV pulse envelope of 1.4 fs. (d), (e) are zoom-ins of the centers of Figs. 1(a) and 1(b). (f), (g) Simulated FROGCRAB data using the optimized values of $D2$ and $D3$, but when the EUV pulse envelope is changed from the optimized value of 1.4 fs to 1 fs and 2.5 fs, respectively. These traces do not match the experimental data.

comparison (dotted black line). Figure 4 shows that the attosecond bursts are broadened from their transform-limited value of 360 as, to a chirped value of 470 as, while the total EUV radiation is contained in an overall intensity envelope of 1.4 ± 0.2 fs FWHM. This corresponds to a single burst with two ~10% sidelobes in the case of a cosine pulse. However, distinguishing a cosine from a sine pulse with two
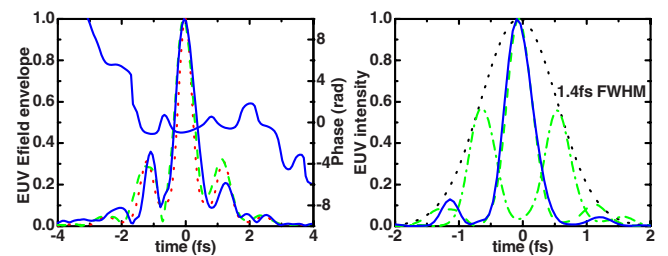

FIG. 4. (Color online) (a) Chirped EUV electric field envelope vs time: (Dashed green line) obtained from optimized fit shown in Fig. 1(b), magnitude (solid blue line) and phase (solid blue line) retrieved from a GP algorithm, and (dotted red line) transform-limited pulse for comparison. (b) (Solid blue line, dashed green line) EUV intensities vs time corresponding to the chirped pulses shown in (a), (dash-dotted green line) intensity of a double pulse with the same envelope, and (dotted black line) intensity envelope of the extracted EUV field.

equivalent intensity bursts [dash-dotted green line in Fig. 4(b)] is not possible. This is because the two FROGCRAB traces are equivalent. To validate the temporal FWHM EUV envelope extracted from our analysis, we also explored the effect of varying the envelope duration in our simulated FROGCRAB traces. We found that varying the pulse envelope also changes the widths and the shape of the FROGCRAB sidebands, as can be seen in the simulated FROGCRAB data for varying EUV pulse envelope in Figs. 3(e), 3(f), and 3(g) for 1.4, 1, and 2.5 fs, respectively. A plot of the rms deviation between the simulated and experimental FROGCRAB traces versus the EUV pulse duration is shown in Fig. 3(c). The best agreement is found for an EUV pulse duration of 1.44 fs (FWHM), in very good agreement with the duration of the EUV field reconstructed from the CCD spectrum for dispersions of $D2 = -0.033$ fs^2 and $D3 = -0.007$ fs^3. Furthermore we checked that including an additional quadratic phase around each harmonic (harmonic chirp [19]) leads to a worse agreement between the data and the fit.

To validate the results of our previous analysis, we performed an independent, unrestricted pulse retrieval using a generalized projection (GP) FROGCRAB algorithm. This algorithm has been adapted to our experimental situation in the same way as was discussed above for the simulated FROGCRAB traces, to take into account photoelectron collection over a 2π solid angle, as well as the addition of two traces for the fundamental pulse—a cosine and minus cosine waveform—by calculating multiple FROGCRAB traces and comparing an appropriately averaged trace to the experimental data. Calculated data are convolved with the photoelectron spectrometer resolution function. The detailed implementation of this algorithm will be the subject of a forthcoming publication. The resulting reconstructed FROGCRAB trace is shown in Fig. 1(c) and shows excellent agreement with the experimental trace. The rms error is 1%. The retrieved temporal electric field profile agrees quantitatively with the one extracted from our first analysis and is shown as the solid blue line in Fig. 4(a). Analysis of the spectral phase of the retrieved electric field (not shown) yields second- and third-order dispersion coefficients $D2 = -0.032$ fs^2 and $D3 = -0.025$ fs^3, in excellent agreement with our first analysis, and in addition shows a small amount of harmonic chirp, but second- (third-) order terms around all harmonics are smaller than 0.1 fs^2 (0.03 fs^3), respectively. Such small amounts of harmonic chirp do not measurably influence the overall EUV pulse envelope, as confirmed by the EUV field retrieved by the GP algorithm, shown in Fig. 4(a), and by the analysis in [19].

Finally, we note that in earlier work [15], simulations predict a dynamically phase-matched gated HHG regime, in which the EUV emission of one harmonic should be localized within an optical cycle, which is consistent with our present measurements. Numerical calculations of single-atom radiation on the other hand, predict EUV pulse durations of 6 fs or longer for our experimental parameters, suggesting the importance of a temporal phase matching that is reducing the EUV pulse duration in our geometry.

In conclusion, we have characterized the amplitude and phase of a complex extreme ultraviolet field with attosecond substructure. Using a hollow-core waveguide geometry we generate sub-optical-cycle pulses from relatively long 13-fs driving laser pulses. Using the FROGCRAB pulse measurement technique, we extracted the extreme ultraviolet wave form consisting of chirped 470-as bursts, spaced by $\sim$1.3 fs, within a 1.4-fs intensity envelope. We also showed that the sub-optical-cycle EUV pulses are near transform limited, with a relatively narrow bandwidth of $\sim$1 eV, making this source ideal for ultrafast state-selective molecular and materials spectroscopy. In this difficult temporal regime, where the laser fundamental cycle of 2.6 fs is comparable in duration to the EUV pulse, we have demonstrated that the FROGCRAB technique can be successfully used to bridge the gap in EUV pulse measurement capabilities between simple noninterferometric crosscorrelation measurements and the RABBITT method, which determines the time structure of individual attosecond bursts, but not the overall envelope. Finally, we have shown that considerable intuition about the EUV pulse characteristics can be obtained directly from the FROGCRAB trace.

---

[1] Rodrigo Lopez-Martens *et al.*, Phys. Rev. Lett. **94**, 033001 (2005).

[2] I. P. Christov, *et al.*, Phys. Rev. Lett. **78**, 1251 (1997).

[3] M. Hentschel *et al.*, Nature (London) **414**, 509 (2001).

[4] P. B. Corkum *et al.*, Opt. Lett. **19**, 1870 (1994).

[5] G. Sansone *et al.*, Science **314**, 443 (2006).

[6] F. He, C. Ruiz, and A. Becker, Phys. Rev. Lett. **99**, 083002 (2007).

[7] E. Gagnon *et al.*, Science **317**, 1374 (2007).

[8] P. Erman *et al.*, Phys. Scr. **62**, 294 (2000).

[9] J. Zobeley *et al.*, J. Chem. Phys. **108**, 9737 (1998).

[10] F. Remacle and R. Levine, Proc. Natl. Acad. Sci. U.S.A. **103**, 6793 (2006).

[11] F. Remacle and R. Levine, J. Chem. Phys. **125**, 133321 (2006).

[12] M. Drescher *et al.*, Nature (London) **419**, 803 (2002).

[13] P. M. Paul *et al.*, Science **292**, 1689 (2001).

[14] Y. Mairesse and F. Quere, Phys. Rev. A **71**, 011401(R) (2005); F. Quere *et al.*, J. Mod. Opt. **52**, 339 (2005).

[15] A. S. Sandhu, E. Gagnon, A. Paul, I. Thomann, A. Lytle, T. Keep, M. M. Murnane, H. C. Kapteyn, and I. P. Christov, Phys. Rev. A **74**, 061803(R) (2006).

[16] A. Rundquist *et al.*, Science **280**, 1412 (1998).

[17] M. Drescher *et al.*, Science **291**, 1923 (2001).

[18] R. Trebino, *Frequency-Resolved Optical Gating: The Measurement of Ultrashort Laser Pulses* (Kluwer Academic, Boston, 2000).

[19] K. Varjú *et al.*, J. Mod. Opt. **52**, 379 (2005).